





D.2.4.1: REPORT & PRESENTATION ON EFFECTIVENESS OF MEASUREMENT SYSTEM & CALIBRATION BASED ON THE PILOT ACTION;

Version 4

02 2025



Project Information

Project ID	CE0100439
Project Acronym	BIM4CE
Project Full Title	Bridge monitoring using real-time data and digital twins for Central Europe
Starting Date	30.03.2023
Duration	3 years
Topic	Strengthening innovation capacities in central Europe
Project Website	https://www.interreg-central.eu/projects/bim4ce/
Project Coordinator	Dr. Ilia Lashkov
Organisation	Technische Universität Dresden
E-mail	Ilia.lashkov@tu-dresden.de
Telephone	+49-351-463-42413

Document Information

Work Package	2
Deliverable Title	REPORT & PRESENTATION ON EFFECTIVENESS OF MEASUREMENT SYSTEM & CALIBRATION BASED ON THE PILOT ACTION
Version	4.0
Contributor(s)	Ilia Lashkov (TUD), Mirko Kosič (ZAG), Andrej Anžlin (ZAG), Doron Hekič(ZAG), Neža Gošte(ZAG), Petra Triller(ZAG), Maja Kreslin (ZAG)
Reviewer(s)	Andrea Piscini (SINA)

Document Classification:									
Draft		Final	X	Confidential		Restricted		Public	

History			
Version	Issue Date	Status	Distribution
1	20.12 2024	Draft	TUD
2	14.01.2025	Draft	ZAG, TUD
3	26.2.2025	Final Draft	All partners
4	27.02.2025	Final	All partners

The information contained in this report reflects the views of the Author(s) and the Commission does not accept responsibility for the use of this information.







Contents

1. Introduction	2
2. Technical data	3
2.1. Leakage monitoring system	3
2.2. Accelerometer-based monitoring system	5
3. Validation of leakage monitoring system at IDA-KI bridge	6
3.1. Description of the validation campaign	6
3.2. Results of the validation campaign	8
3.3. Conclusions of the validation campaign	12
4. Validation of the accelerometer-based monitoring system at ZAG's laboratory	12
4.1. Description of the validation campaign	12
4.2. Results of the validation campaign	15
4.3. Conclusions of the validation campaign	21
5. Conclusions and further steps	22
References	23







1. Introduction

The Deliverable 2.4.1: Report & Presentation on the Effectiveness of the Measurement System and Calibration is based on the requirements and specifications from WP1, as well as the information collected from Activity 2.2. A demonstration of the designed measurement system was conducted on two independent sites. In parallel with the leakage sensor tests performed by TU Dresden on the IDA-KI bridge, ZAG benchmarked the capabilities of the accelerometer-based bridge monitoring solution in detecting and predicting structural damage in their laboratory for structural testing.

This IDA-KI bridge is designed as a full-scale open laboratory to test different monitoring solutions and, as such, offers a unique opportunity for testing and validating equipment under real-world conditions. The research bridge "IDA-KI" was constructed in the summer of 2022 near the lead partner, the Dresden Integrated Center for Applied Physics and Photonic Materials, as part of a project funded by mFUND and the German Federal Ministry of Transport and Digital Infrastructure (BMVI). All relevant stakeholders have agreed to use the bridge for testing, including the builder, Hentschke Group, which has close ties to TU Dresden.

The validation at ZAG's Laboratory for Structures provides a unique opportunity to test the monitoring solution in a controlled environment, leveraging advanced laboratory capabilities that enable structural elements to be tested up to their failure. To assess the effectiveness of accelerometer-based bridge monitoring in detecting structural damage, two full-scale bridge beams - salvaged from a real bridge before its decommissioning - were tested up to failure. The results were used to correlate known structural damage with changes in the beams' natural frequencies recorded by the monitoring system. These frequency changes serve as indicators of bridge deterioration, enabling early warnings of abnormal behaviour and supporting proactive maintenance.

The measurement system developed in Activity 2.2 was tested under these controlled yet realistic conditions, yielding a unique dataset. This dataset enables validation and demonstrates the system's adaptability to meet end-user requirements.

This report includes the measurement results from the leakage sensors tested on the IDA-KI bridge and the vibration tests conducted in ZAG's full-scale structural testing facility.







2. Technical data

2.1. Leakage monitoring system

The water leakage sensor is a flexible film designed to generate a signal upon contact with water. It is connected to a secure power supply, eliminating any risk of electrical contact. The Technical characteristics of leakage sensor foil are shown in more detail in Deliverable 2.2.1, a Data sheet with technical specifications of sensor foils, which includes technical specifications and explanations on how this data was derived.

The sensor foil has a thickness of 125 μ m and a tensile strength of 260 MPa. Its elongation at break is 100%, while shrinkage at 150 °C is 0.2% in longitudinal and 0.3% in transverse directions. In real conditions with various humidity ranges, the foil operates within a temperature range of -10 °C to 120 °C.

The measurement principle relies on changes in the sensor's capacitance when exposed to varying volumes of water. Figure 1 illustrates the correlation between the change in capacitance and the detected water volume. The sensor achieves a maximum resolution of 0.1 mL for water droplets on the sensor. We increased the maximum volume to 100 mL, at which point the water forms a continuous layer, fully covering the sensor. However, such a high resolution for water detection is unnecessary for the bridge application. As demonstrated in our measurement tests (presented in the Experimental Data Section), the sensitivity of the leakage sensor foil should be adjusted to allow for the measurement of larger amounts of leakage while minimising noise caused by humidity.

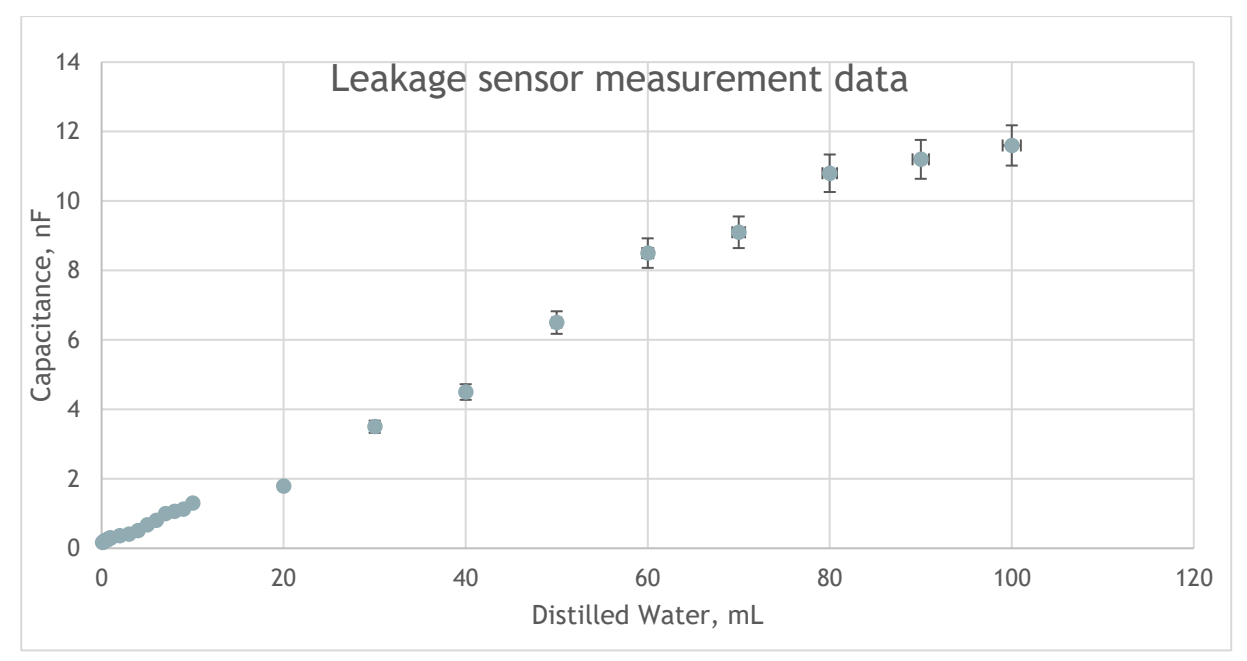


Figure 1. Calibration relationship of the leakage sensor







The leakage sensor is connected to an acquisition system that collects sensor data and converts it into a digital signal. The signal is transmitted using various technologies to a data storage server. TU Dresden developed the acquisition system, which allows simultaneous measurement from seven leakage sensors. The size of the sensors and the threshold values for measurement can be adjusted as needed.

The system is fully assembled in-house using components sourced from external suppliers. Additionally, TU Dresden has developed and integrated embedded software to ensure stable data acquisition and transmission via IoT, which is incorporated into the circuit board.

The specifications of the acquisition system, designed specifically for the leakage sensor foils, are presented and explained in Table 1.

Table 1. Specification of acquisition system developed at TU Dresden for BIM4CE project.

Parameter	Specification		
Power Supply	12V DC, 500mA		
System Components	 ESP32-based readout circuit Raspberry Pi for data storage and processing 		
Data Transfer	USB Serial Communication between the readout circuit and Raspberry Pi		
Sensor Interface	Ethernet cable (CAT5e or higher model) with RJ45 connector		
Maximum Sensor Capacity	7 sensors		
Sensor Input Type	Pulse signals (rising edge)		
Pulse Counting Interval	1 second		
ESP32 GPIO Characteristics	Max GPIO frequency: 40 MHz (depending or configuration)- Input Voltage Range: 0V to 3.3V		
Pulse Counting Accuracy	Determined by the ESP32 timer precision (within microseconds)		
RJ45 Ethernet Pinout	Standard TIA/EIA-568-B wiring for sensor input		
Storage Capacity	Determined by Raspberry Pi storage (e.g., SD card)		
Data Logging Rate	1 log per second per sensor (adjustable via firmware if required)		
Communication Protocol	USB Serial: 115200 baud rate		
System Dimensions	15 cm × 12 cm × 7 cm		
Ambient Operating Conditions	Temperature: -20°C to 85°C (ESP32 operational range)		
Firmware Update Mechanism	USB or Over-the-Air (OTA) for ESP32		
Safety Features	Over-voltage protection on ESP32 input		







2.2. Accelerometer-based monitoring system

The DEWESoft structural health monitoring solution was [1] used for accelerometer-based monitoring during the testing campaign at ZAG's laboratory. The system is based on the industrial EtherCAT communication protocol, which allows the sensors to be daisy-chained with a single inexpensive CAT6 cable providing power, data transfer and synchronisation (down to 1 ms) up to 100m device-to-device distances.

The acceleration-based monitoring system was composed of two types of accelerometers, i.e. the MonoDAQ-E-gMeter and the more sensitive IOLITEi-3xMEMS-ACC-s (Figure 2). The MonoDAQ-E-gMeter is a predecessor of the current IOLITEi-3xMEMS-ACC series and is a fully integrated low-noise 3-axial MEMS accelerometer with EtherCAT interface. The IOLITEi-3xMEMS-ACC-S is a more sensitive version of the sensor with a spectral noise density of just 0.7 μ g//Hz compared to 25 μ g//Hz of the MonoDAQ-E-gMeter. This allows for the detection of even smaller acceleration ranges. The technical specifications of the employed accelerometers are summarized in Table 2.



Figure 2. Employed accelerometers: MonoDAQ-E-gMeter (left) and IOLITEi-3xMEMS-ACC-S (right) [2]

Table 2. Specification of acquisition system for accelerometers

. 45 10 21 5 5 5 5 11 15 41 15 11 15 15 15 15 15 15 15 15 15 15 15	ion system for accelerometers		
	MonoDAQ-E-gMeter	IOLITEI-3xMEMS-ACC-S	
Nr. of axes	3	3	
Measurement ranges	±2 to ±8g	±15g	
Max. sampling rate	4 kS/s	1 kS/s	
Bandwidth at max. sample rate	0 1000 Hz	0 460 Hz	
Dynamic range at max. bandwidth	96 dB	137 dB	
Noise spectral density	25 μg/√Hz	0.7 μg/√Hz	
Digital interface	EtherCAT	EtherCAT	
Interface connectors	RJ45	RJ45	
Power consumption	1300 mW	1500 mW	
Supply voltage	12-48 V	12-48 V	
Operating temperature	-20°C 50°C	-40°C 65°C	
IP rating	IP20	IP20	
IP67 option	\checkmark	✓	
Weight	105 g	155 g	
Dimensions	82.7 x 68 x 22.3mm	82.7 x 68 x 37.4mm	
Weight IP67 chassis	700 g	900 g	
Dimensions IP67 chassis	132 x 72 x 40mm	132 x 72 x 49mm	
Housing material	Aluminium	Aluminium	







3. Validation of leakage monitoring system at IDA-KI bridge

3.1. Description of the validation campaign

The system for testing the leakage sensor foils consisted of 1-meter-long leakage sensor foils and a specially developed acquisition system for monitoring leaks using them. The system was installed on the IDA-KI bridge on **December 4, 2024**, and measurements of the bridge's leaks were taken on **December 12, 2024**.

The location for sensor installation was chosen based on recommendations from Hentschke Group engineers, who built the bridge and identified areas with potential leaks during snow or rain.

Additionally, a weather station was used to collect external environmental data. The following parameters were monitored:

- Rain sensors (mm/min): To detect possible leaks, analyse delays, and determine how much rain could cause the bridge to leak.
- Solar radiation (W/m²): To evaluate the drying of the bridge surface.
- Air humidity (%RH): To analyse whether the leakage sensors are sensitive to humidity or dew formation.
- Air temperature (°C): To assess whether the sensors measure water or ice and to evaluate the likelihood of water freezing overnight and melting during the day, potentially causing leaks.

The weather station was positioned on top of the bridge, while the leakage sensor foil was installed underneath the bridge, the deck, and the girder to prevent direct contact with rain and sunlight. This setup is shown in Figure 3.

The acquisition system was enclosed in a waterproof case, and other sensors were used on the bridge. The system was powered by a 220V power supply, converted to DC 12V using an adapter, as shown in Figure 4.









Figure 3. Installation of leakage sensor foil under the bridge



Figure 4. Case with data acquisition systems







The acquisition sensor was designed to detect leakages by measuring the oscillation frequency. To minimize noise interference, the threshold leakage values can be set manually, depending on the size of the sensor foil, its capacitance values, and the amount of leakage.

In our measurement data, the frequency dropped to 100 Hz, indicating the occurrence of a leakage.

We integrated multiple leakage sensors, each 20 cm long, connected in series on a single foil to enhance measurement accuracy. This configuration helps mitigate potential malfunctions of individual sensors and better detect leakage distribution.

3.2. Results of the validation campaign

The initial values measured by the leakage sensors are capacitances. However, the logging system developed at TU Dresden records the final measurement as frequency, which is the inverse of the capacitance value. When the sensor foil comes into contact with a leak, the system's capacitance increases, causing the oscillation frequency to decrease.

In the measurement graph, we illustrate how the frequency changes, but for simplicity, we omit the actual frequency values. Instead, we represent the measurements as dots: when the sensors are in a dry state, the values remain high, and as soon as water reaches the sensor, the values drop to a minimum, reaching the measurement threshold.

The graphs below show the measurements from a single sensor foil containing sensors 2, 3, 4, and 6, each assigned a distinct color. Measurements were taken over 8 dates, but for clarity, we present only the first 3 dates, as they are the most representative of the results.

Day 1. 04.12.2024

- 10:30: The sensor was installed.
- 10:45: The measurement system was tested by pouring water along the sensor foil. This test is indicated by the lowest value at 100 Hz frequency as shown on the graph as a minimum value line.
- 15:30 16:30: It rained at a rate of 0.04 mm/min for one hour. The leakage detection showed a delay of approximately one hour, and the sensor indicated that the foils remained wet until the end of the day. The humidity also went above 90% as the rain started.
- **18:00:** The sensor showed no leakage detection up to this point, confirming a period of stability after the initial test.
- 19:00 20:00: It rained again at a rate of 0.05 mm/min for one hour. The bridge continued to leak after this second rain event, as detected by the sensor.







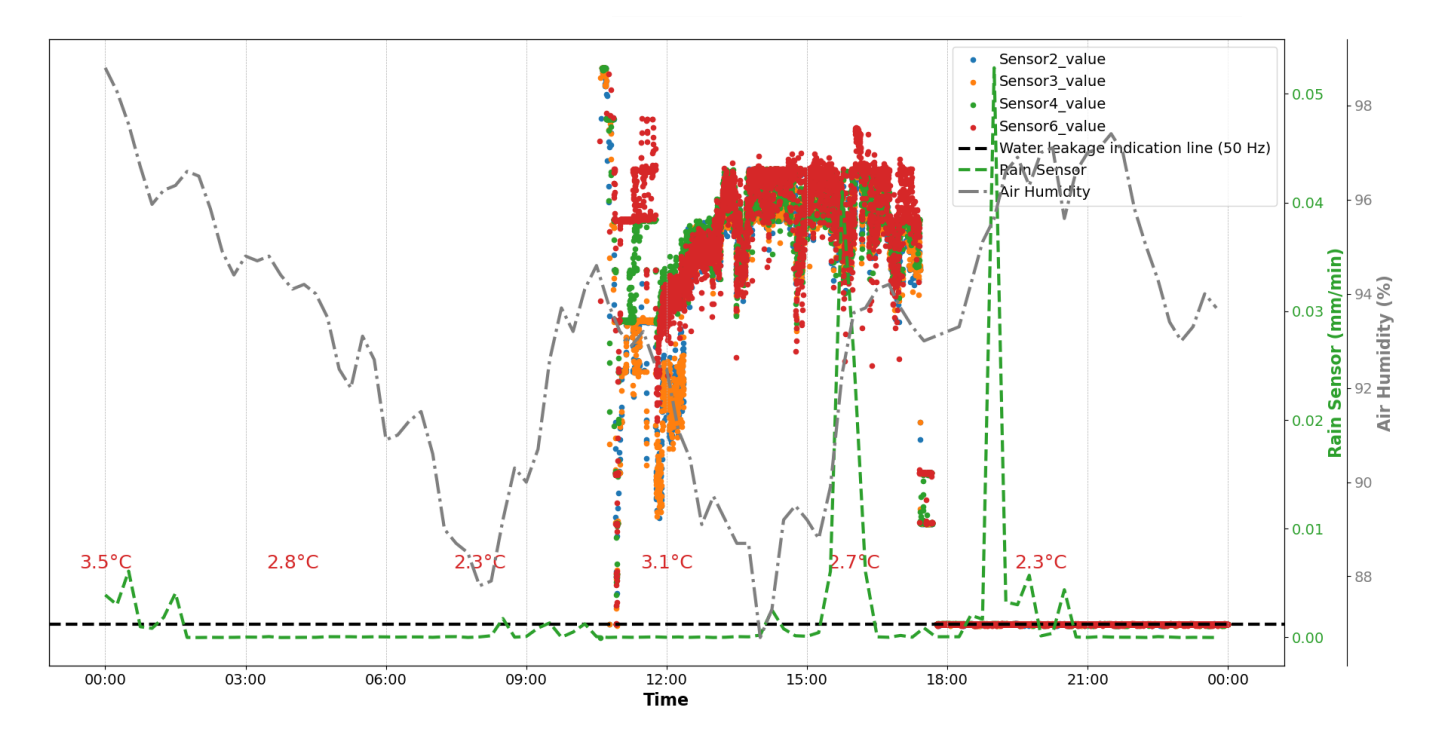


Figure 5. Day 1 of measurement.

Day 2. 05.12.2024

- 3:00 AM: The day began with heavy rainfall at a rate of 0.08 mm/min, which lasted for approximately 30 minutes.
- 10:00 AM: Air humidity sensors recorded levels above 80% until this time.
- 12:00 PM: Humidity dropped to 65% and fluctuated between 60% and 85% for the rest of the day. This marked the beginning of the drying process on the bridge.
- **6:00 PM:** The sensors indicated no further leakage from this time onward, as the residual water from the morning rain had dried out.
- End of the Day: The sensor readings remained stable, confirming the absence of leaks for the remainder of the day.







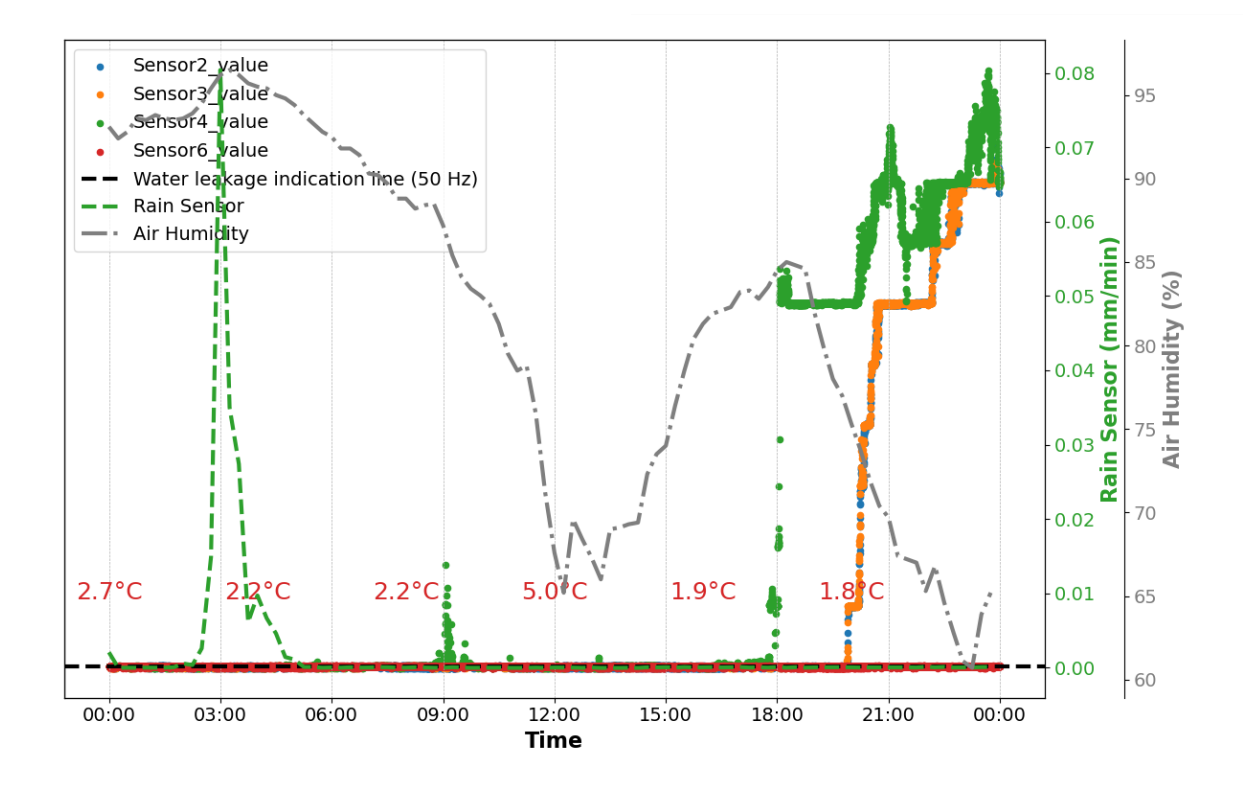


Figure 6. Day 2 of measurement.

Day 3. 06.12.2024

- **2:00 AM:** The sensor began detecting leakage, suggesting water had started accumulating under the bridge.
- 3:00 AM: Air humidity began to rise sharply from 65% to 85% in less than an hour.
- **4:00 AM:** Strong showers were observed, with rainfall intensity reaching 0.03mm/min.
- 7:00 AM 12:00 PM: Heavy rainfall continued, with rates exceeding 0.06 mm/min.
- **Subsequent Days:** Water remained trapped between the bridge and the leakage sensors, as indicated by the sensor data.

The sharp increase in air humidity at **3:00** AM, coupled with intense rainfall events at **4:00** AM and sustained heavy rain between **7:00** AM and **12:00** PM, created conditions for significant water accumulation. The sensors effectively detected leakage starting at **2:00** AM, demonstrating early sensitivity to water presence. However, the water became trapped between the bridge and the sensors, leading to prolonged leakage indications in the following days.







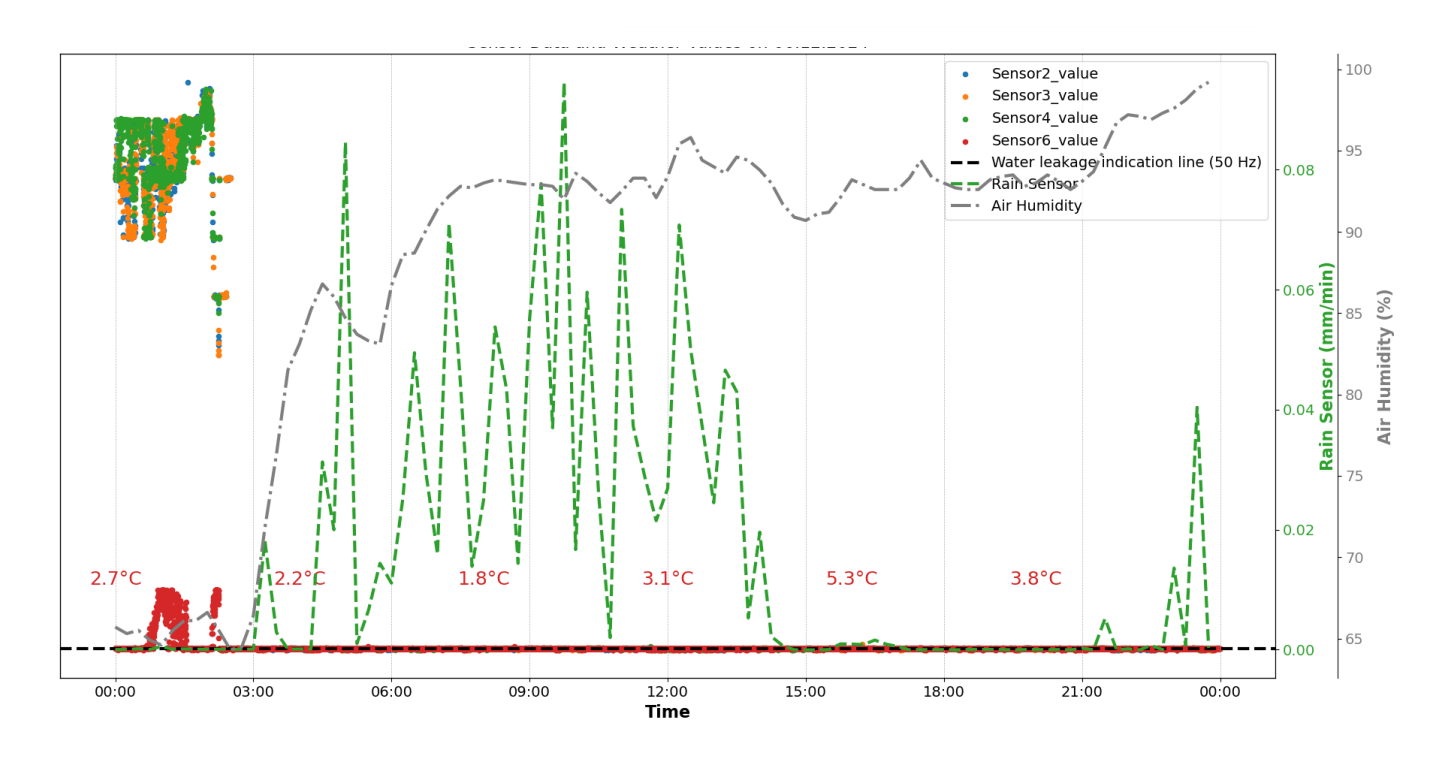


Figure 7. Day 3 of measurement

Combined graph of all three days:

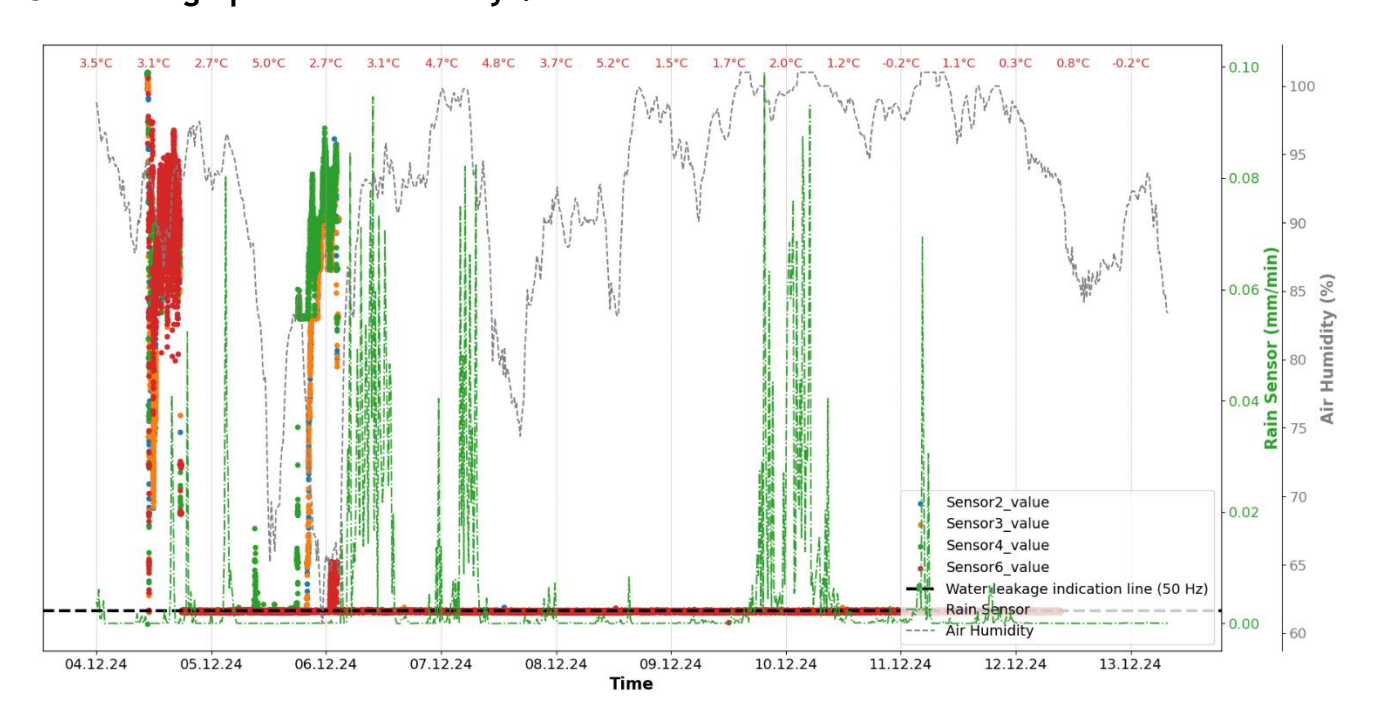


Figure 8. All days of measurement together







3.3. Conclusions of the validation campaign

Sensor 6 was the last sensor and was located directly beneath the hole where the leak occurred. This observation aligns with the measurement data, which shows that after the first day of heavy rain, Sensor 6 consistently indicated the presence of trapped water between the foil and the bridge, while Sensors 2, 3, and 4 showed an operational status, indicating the periods when the leak had stopped and the sensor foil, along with the surface it was attached to, had dried. However, we also observed that the sensor foil was highly sensitive and could indicate a leak shortly before heavy rain, when air humidity reached 90% and precipitation began. To mitigate this, further measurements will be conducted using larger sensor foils with a less sensitive configuration to avoid false leak indications caused by high humidity or minor water accumulation. These measurements will be performed in an environmental chamber at TU Dresden, where temperature and humidity can be controlled. This setup will help confirm that the sensor foils do not falsely indicate leaks due to high humidity alone, except when condensation forms on the surface. Additionally, an upcoming experiment on the IDA-KI bridge will use two less sensitive leakage sensor foils placed at different locations, both exposed to potential leaks. This approach will allow us to compare the measurement data and improve reliability.

To conclude, the leakage detection system demonstrated a reliable ability to detect leaks on the bridge, with measurements aligning closely with weather station data, including rainfall events. The system successfully detected leaks even in challenging conditions and remained operational at temperatures below freezing.

4. Validation of the accelerometer-based monitoring system at ZAG's laboratory

4.1. Description of the validation campaign

The validation of the accelerometer-based bridge monitoring was performed in the Laboratory for Structures at the Slovenian National Building and Civil Engineering Institute (ZAG), where two full-scale bridge beams were tested up to failure. The bridge beams were salvaged from a real bridge, which was damaged and removed following the devastating floods in Slovenia in August 2023. The primary objective of the tests was to evaluate the effectiveness of accelerometer-based monitoring in detecting structural damage based on changes in dynamic properties, such as natural frequencies. This chapter first presents the bridge and the tested beams, followed by a detailed description of the test setup and loading protocol.

The bridge was designed in 1947. It was located on a state road in Slovenia. The total length of the bridge was 52.60 m, divided into five spans with lengths of







9.30 + 10.50 + 13.00 + 10.50 + 9.30 meters. The width of the bridge was 8.20 meters. The original superstructure was ribbed reinforced concrete (RC) slab with 70 cm thick brick inserts. The intermediate supports were 30 cm thick and 5.30 m high walls. The abutments were massive with parallel wings.

In the year 1989 the bridge was widened to accommodate additional lanes for pedestrians and cyclists. The bridge expansion was made with two prestressed beams on the left and right side of the existing bridge. The construction was made using prefabricated prestressed RC T-beams. These were placed on additional thin wall intermediate supports aligned with the previous supports. T-beams were 70 cm high, with the width of the top flange of the beams 1.10 m. Beams were 3 cm apart and were interconnected at the top with an 18 cm thick RC slab. Schematic presentation of existing bridge with subsequent extension is shown in Figure 99.

After the bridge replacement, several beams from the bridge expansion were transported to ZAG for further testing. Two of these beams were selected for the study. The cross-section of the tested T-beams is shown in Figure 10. The beams have a total length of 10.50 m and a span length is 9.90 m.

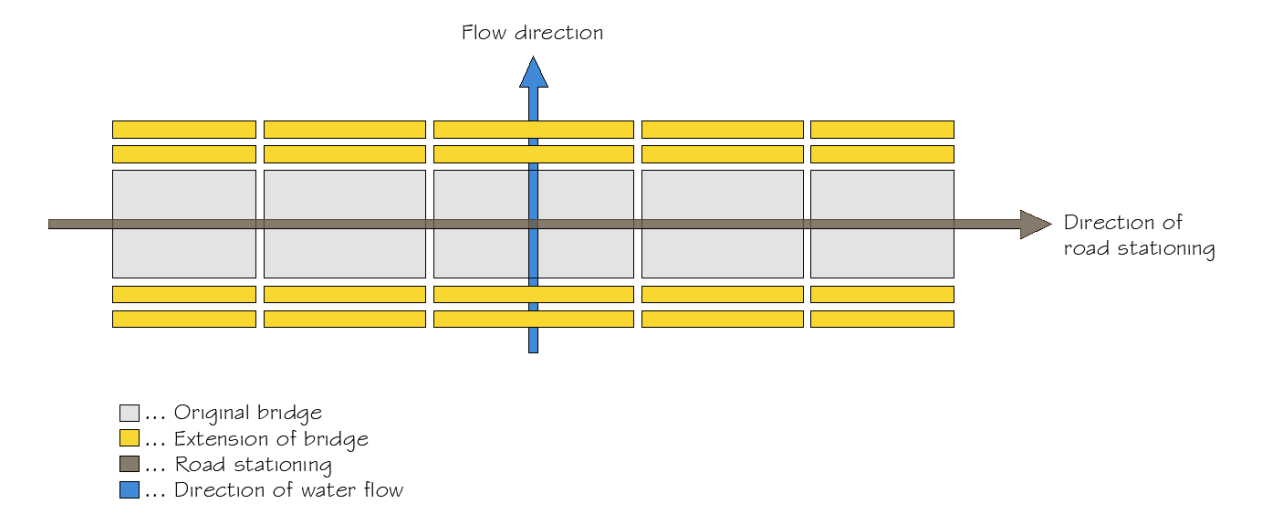


Figure 9. Schematic representation of a bridge with subsequent extension.

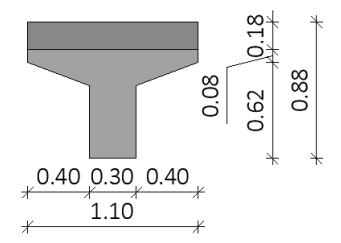


Figure 10. Cross section of tested beams with RC slab on top.









The beams were constructed using concrete MB40 (approximately C35/45 according to Eurocode 2), while all other RC elements, including the deck, were made of concrete MB30 (approximately C25/30). The reinforcement used was prestressed cables 1840/2090 MPa (f_{sy} = 1840 MPa), smooth rebar GA 240/360 (f_{sy} = 240 MPa), ribbed rebar RA 400/500 (f_{sy} = 400 MPa) and mash reinforcement MAG 500/560 (f_{sy} = 500 MPa).

The test setup is shown in Figure 11. The beam was simply supported with pinned support on one and roller support on the other side. The supports were rigidly fixed to the laboratory's strong floor. The beam was laterally supported by a rigid steel frame. The load on the beam was applied by a hydraulic actuator, which was clamped into the steel structure.

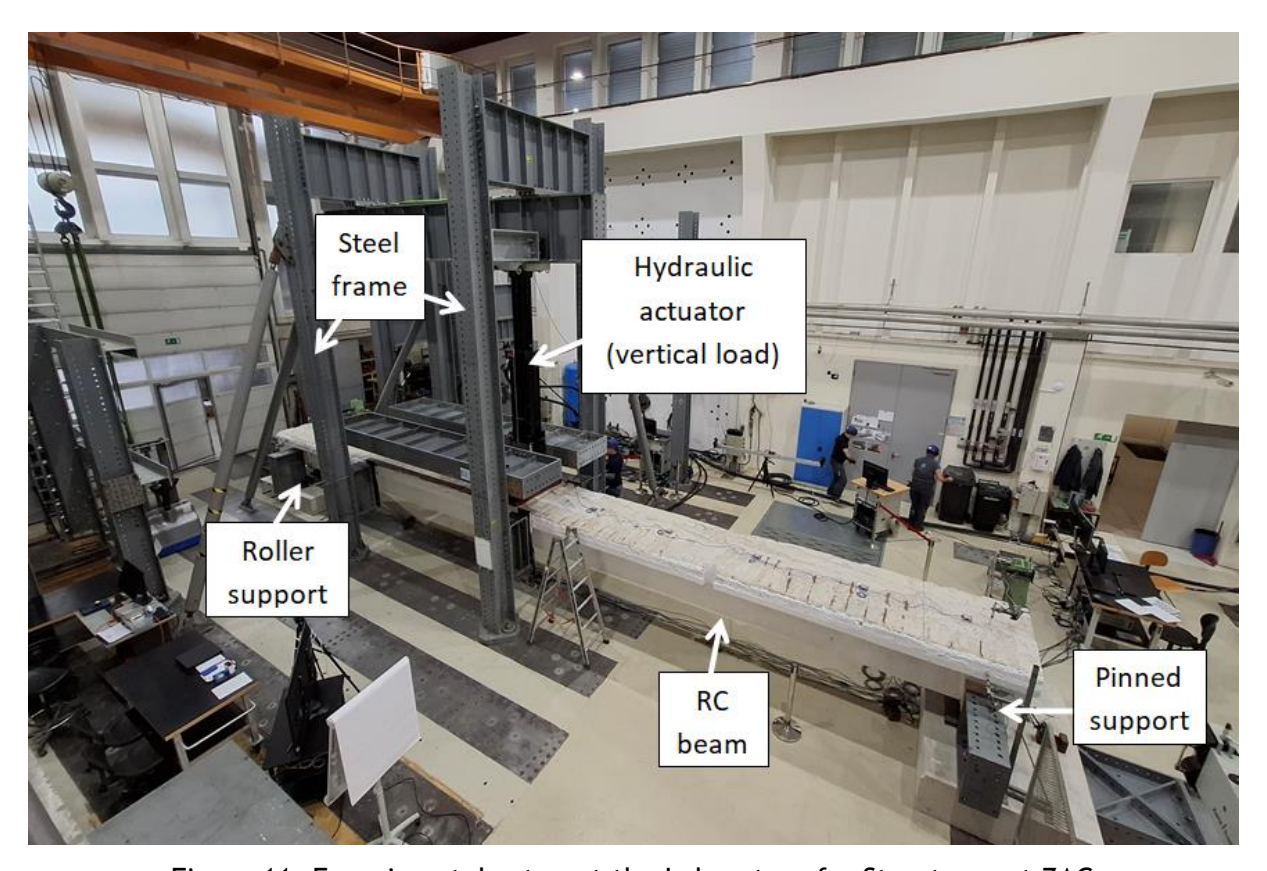


Figure 11. Experimental setup at the Laboratory for Structures at ZAG

The beam instrumentation, crucial for validating the dynamic characteristic measurements, included a force transducer, a displacement transducer and accelerometers. The latter are shown in Figure 12. Static cyclic flexural tests were performed. The vertical force was applied in the middle of the beam.







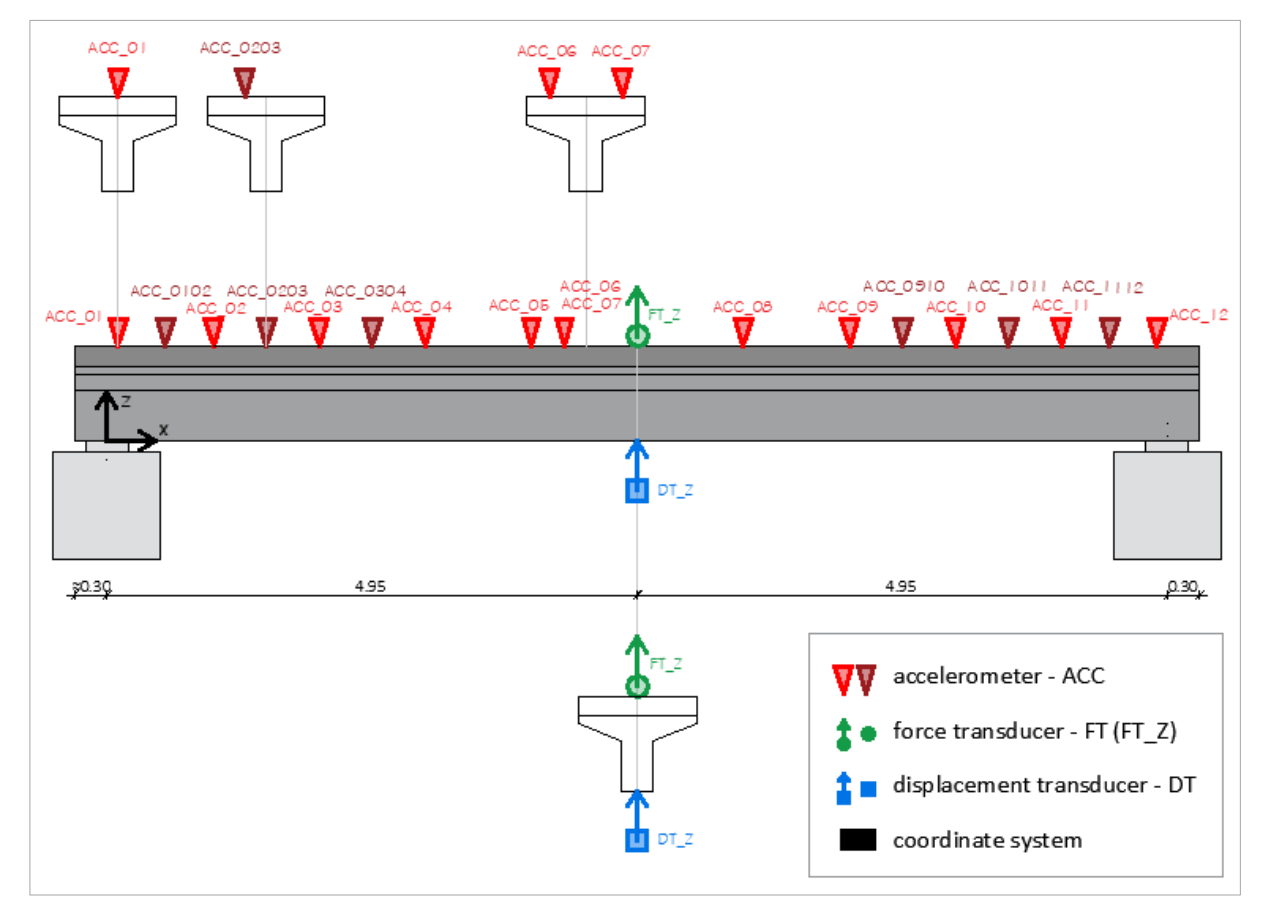


Figure 12. Instrumentation.

The testing procedure generally consisted of 2 stages. In the first stage, the force was controlled, and in the second step, the displacement was controlled. Each stage consisted of individual phases, which were defined by the force (step 1) or displacement (step 2), where each individual phase consisted of 2 identical cycles. With each phase, the load (force or displacement) increased until the beam collapsed.

4.2. Results of the validation campaign

This chapter presents the results of the flexural tests of two beams, B1 and B2. Beam B1 was tested without the top RC slab, while beam B2 included the RC slab but was intentionally weakened before testing by cutting through 30% of the prestressing cables. This provided an additional damage situation, on top of which further cyclic load tests were performed.

Experimentally obtained hysteretic curves, which describe the relationships between the imposed force and displacement for both specimens, are shown in Figures 14 and 14. To compare the behaviour and analyse the differences, the force and displacement, as well as some other characteristics of the tested beams, have been evaluated at four limit states, namely:







- LS1: crack state representing the maximum load in the phase where first cracks appear, but still close after unloading.
- LS2: before yield state representing the maximum load in the phase where reinforcement has not yet yielded, but cracks are visible upon unloading (permanent cracks).
- LS3: yield state representing the maximum load in the phase where reinforcement has yielded, and large cracks are visible upon unloading.
- LS4: near collapse state representing the maximum load in the penultimate phase before failure.

The damage to both beams during the test is described below.

B1: The first cracks appeared in the 2nd loading phase. They developed in the load application zone, with an initial width of 0.1 mm. After unloading, the cracks fully closed. In subsequent phases, as the load increased, the cracks widened and branched further, increasing their number and distribution. In areas closer to the supports, inclined (shear) cracks also began to form. In the phase just before failure, the maximum crack width reached 4.5 mm, with 3.0 mm remaining after unloading. In the next phase, flexural failure of the beam occurred, accompanied by rupture of the prestressing cables at the load application zone.

B2: Before the flexural test, the beam was intentionally weakened by cutting the lower row (30%) of prestressing cables near the load application zone. The first cracks appeared in the 2nd loading phase. They developed in the weakened section, their maximum width was 0.4 mm. After unloading, the crack width measured 0.1 mm. In subsequent phases, as the load increased, the cracks widened and branched further, increasing their number and distribution. In areas closer to the supports, inclined (shear) cracks also began to form. In the phase just before failure, the maximum crack width under applied load reached 5.0 mm, with 3.0 mm remaining after unloading. In the next phase, flexural failure of the beam occurred at the weakened section, where the remaining prestressing cables ruptured.

Some crucial information defining the beam behaviour at the abovementioned limit states is presented in Tables 3 (B1) and 4 (B2). The corresponding damage states for both beams at LS1 and LS4 are shown in Figure 15. Tables 3 and 4 also include the limit state displacement ratio (d_{LS}/d_{max}) , which quantifies the severity of the damage state relative to the specimen's displacement at maximum load in last phase, denoted as d_{max} . (see Figures 14 and 14).







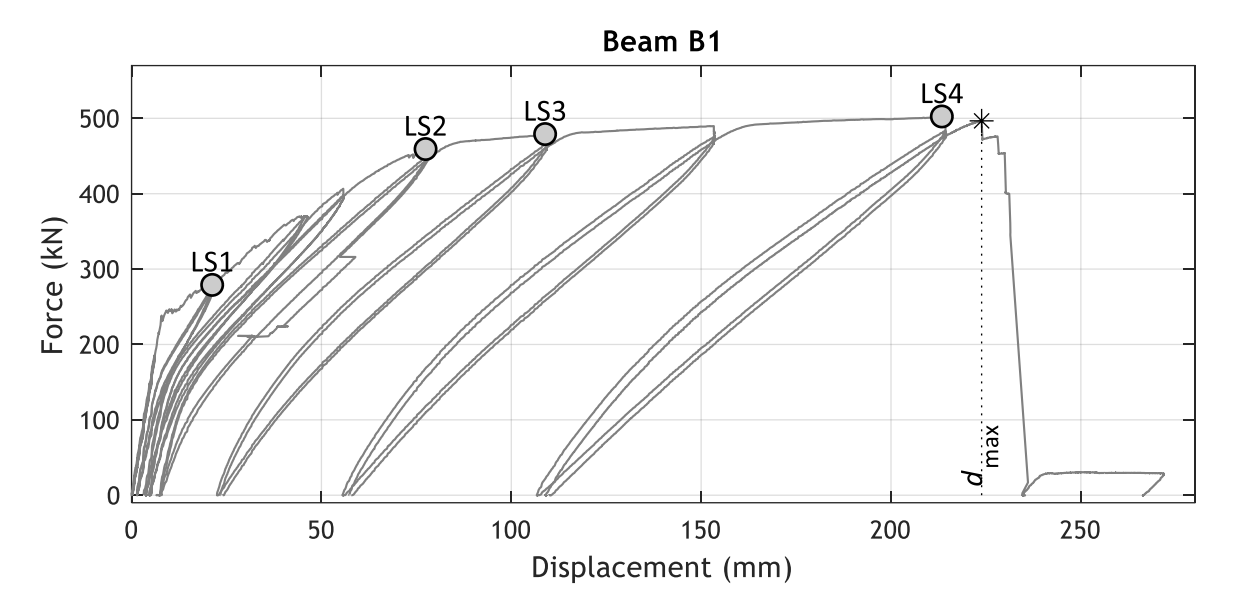


Figure 13. Hysteretic response of beam B1

Table 3. Information defining the beam B1 behaviour at defined limit states (LS).

B1	Displacement [mm]	Force [kN]	Crack width at maximum load [mm]	Crack width at after unloading [mm]	Displacement ratio d_{LS}/d_{max}
LS1: crack	21.5	277.7	0.1	0.0	0.10
LS2: before yield	77.7	458.0	0.8	0.1	0.35
LS3: yield	109.2	477.8	1.8	0.5	0.49
LS4: near collapse	213.7	501.2	4.5	3.0	0.95







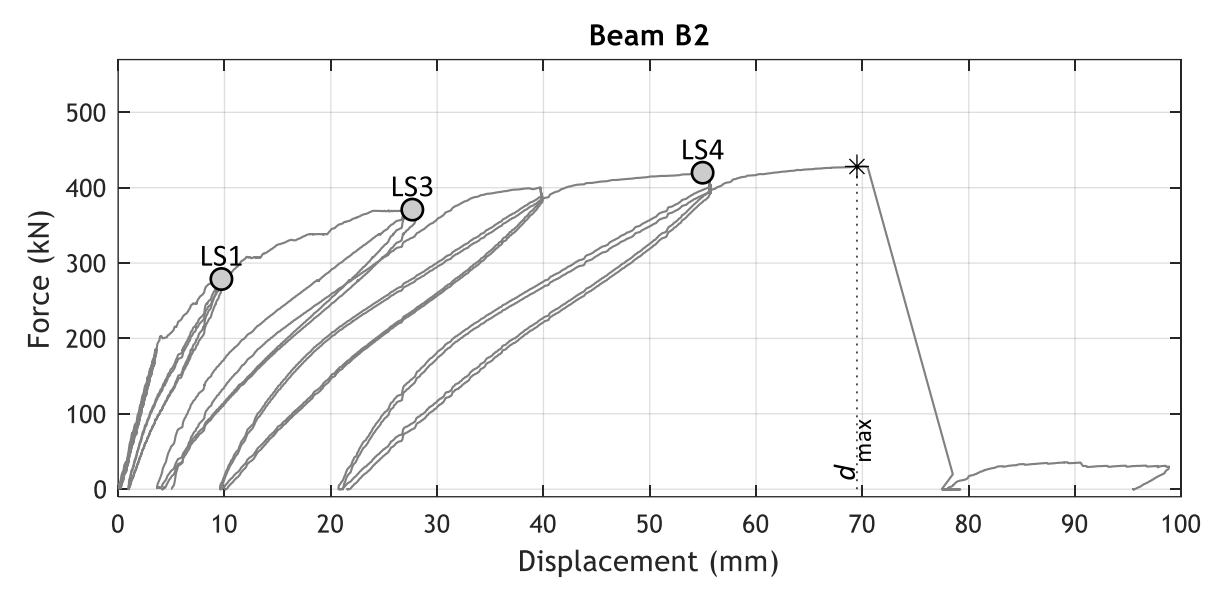


Figure 14. Hysteretic response of beam B2

Table 4. Information defining the beam B2 behaviour at defined limit states (LS).

B2	Displacement [mm]	Force [kN]	Crack width at maximum load [mm]	Crack width at after unloading [mm]	Displacement ratio d _{LS} /d _{max}
After cutting of cables	/*	/	/	/	/
LS1: crack	9.8	277.5	0.4	0.1	0.14
LS2: before yield	/	/	/	/	/
LS3: yield	27.8	369.6	1.6	0.2	0.40
LS4: near collapse	55.1	418.6	5.0	3.0	0.79

^{*} The changes detected in the displacement measurement were within the measurement accuracy.









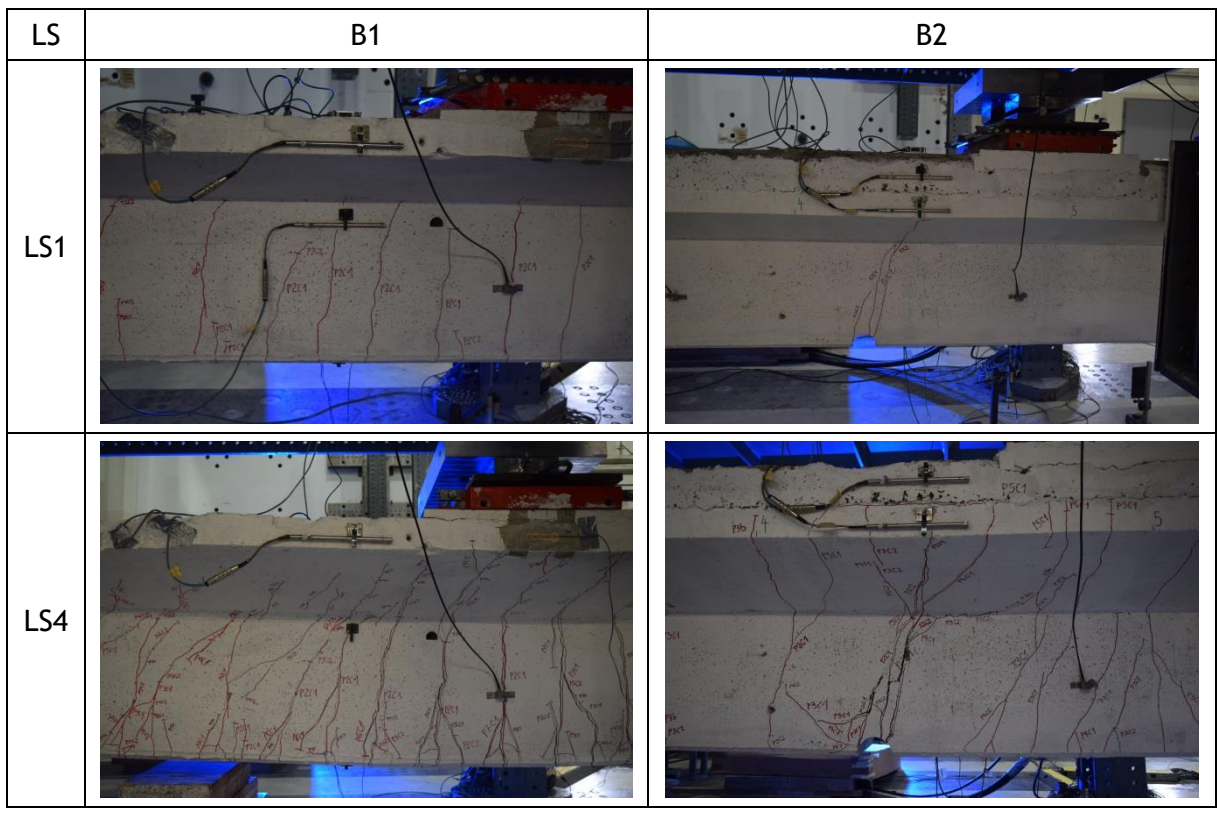


Figure 15. Damage to the beam in the load application zone for limit states LS1 and LS4 for specimen B1 (left column) and B2 (right column)

Acceleration-based monitoring for damage detection was validated through ambient vibration measurements after each characteristic experimental phase. During these measurements, the beams were fully unloaded to maintain the initial boundary conditions. The reference state of the undamaged beams was first established to assess changes in dynamic characteristics under different damage scenarios.

Ambient vibration measurements were performed using Operational Modal Analysis (OMA) implemented in the software DEWESoft ARTeMIS OMA [3]. This enabled the estimation of key dynamic characteristics, including natural frequencies, mode shapes, and damping. Only the natural frequencies of the first two vertical bending modes are analysed in this study. A schematic representation of the mode shapes is shown in Figure 16 for the example of Beam 1, while Tables 5 and 6 summarise the changes in natural frequencies throughout the experimental phases.







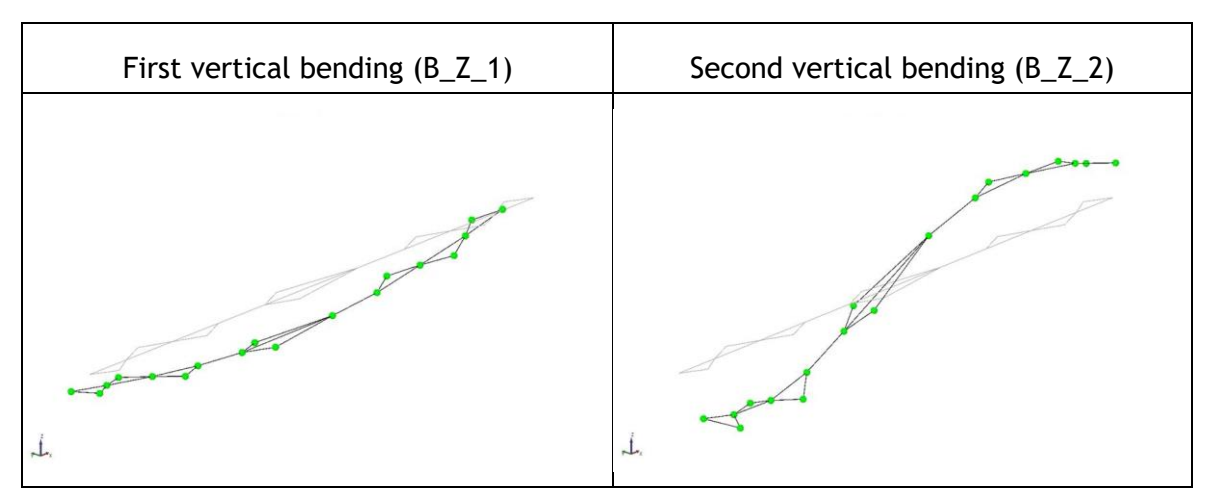


Figure 16. First and second vertical bending modes of the Beam 1.

The reference natural frequencies of Beam 1 were 12.38 Hz and 45.81 Hz for the first and second vertical bending modes, respectively (Table 5). Slightly higher frequencies were observed for Beam 2, at 14.69 Hz and 46.99 Hz (

Table 6), indicating increased stiffness of the beam due to the presence of the top slab.

Damage to the beams reduces their stiffness, as evidenced by a decrease in natural frequencies. This trend is clearly observed in Tables 5 and 6, where increasing damage severity leads to progressively greater frequency reduction. For example, in Beam 1, the formation of the first cracks caused a decrease of approximately 19% and 4% in the first and second natural frequencies, respectively (Table 5). At the near-collapse limit state, these drops reached nearly 50% and 15%. Beam 2 exhibited significantly lower sensitivity (see

Table 6), with comparable limit state classifications still resulting in substantial frequency reductions. This difference is likely due to variations in damage distribution. As shown in Figure 15, cracking in Beam 2 is concentrated at a weakened spot, limiting stiffness reduction to a narrow region. In contrast, damage in Beam 1 is more widespread, leading to a greater overall stiffness reduction. Consistent with this observation, cutting the cables in Beam 2 had a negligible impact on its frequency, as the stiffness reduction was limited to the damaged area. This behaviour is characteristic of bonded prestressed beams, where cable damage causes only a localized loss of prestressing while the prestressing force remains unaffected elsewhere.

Damage had a greater impact on the first vertical bending mode than on the second. This is due to the applied load causing more damage near midspan, where









the first bending mode exhibits its highest amplitude. In contrast, the second bending mode was less affected, as its amplitude near midspan is close to zero.

Table 5. Change in mode shape natural frequencies during experimental phases (Beam 1)

	Natural fre	quency [Hz]	Relative o	change [%]
B1	First vertical bending (B_Z_1)	Second vertical bending (B_Z_2)	First vertical bending (B_Z_1)	Second vertical bending (B_Z_2)
Reference	12.38	45.81	\	\
LS1: crack	11.95	45.15	-18.7	-3.9
LS2: before yield	11.50	44.31	-21.7	-5.7
LS3: yield	10.34	43.81	-29.6	-6.8
LS4: near collapse	7.95	40.83	-45.9	-13.1

Table 6: Change in mode shape natural frequencies during experimental phases (Beam 2)

	Natural free	quency [Hz]	Relative o	change [%]
B2	First vertical bending (B_Z_1)	Second vertical bending (B_Z_2)	First vertical bending (B_Z_1)	Second vertical bending (B_Z_2)
Reference	14.69	46.99	\	\
After cutting of cables	14.64	46.73	-0.3	-0.6
LS1: crack	14.33	46.24	-2.5	-1.6
LS3: yield	13.75	46.22	-6.4	-1.6
LS4: near collapse	11.6	45.58	-21.0	-3.0

4.3. Conclusions of the validation campaign

The validation campaign results demonstrate the capability of acceleration-based monitoring for detecting structural damage through changes in a bridge's natural







frequencies. Results suggest that the frequency decrease depends on the extent of the damage attained during the text. Namely, a wider extent of the damage (of approximately similar magnitude) resulted in a larger decrease in natural frequencies. In both specimens, the acceleration-based monitoring detected even small levels of damage, such as the formation of the first cracks. It should be noted, however, that the demonstration was conducted under controlled laboratory conditions with constant temperature. In real-world applications, environmental factors, particularly temperature fluctuations, can affect structural response and complicate damage detection. Therefore, in further studies, more focus should be put towards implementing tracking temperature-normalized frequency changes.

Additionally, this study primarily examined changes in natural frequencies as a proxy for damage detection, whereas mode shape variations could provide further insights. Therefore, future work is needed to explore this aspect and enhance the reliability of damage detection methodologies.

5. Conclusions and further steps

The validation of leakage sensors at the IDA-KI bridge provided a valuable opportunity to test the system's performance under controlled yet realistic conditions. The results suggest that the sensor located directly at the leak site consistently detected trapped water between the foil and the bridge. To improve accuracy, future measurements should utilize larger sensor foils with a less sensitive configuration and alternative coating materials to isolate the electrodes from moisture, minimizing interference from humidity fluctuations and minor leaks. Future experiments in the environmental chamber at TU Dresden will be conducted to analyze optimized sensor foil configurations, followed by additional field tests on the IDA-KI bridge to validate the findings. In summary, the leakage detection system demonstrated reliable performance, correlating closely with weather station data and effectively detecting leaks on the bridge, even in challenging conditions such as subzero temperatures.

The validation of the accelerometer-based bridge performed in the ZAG's Laboratory for Structures confirmed the potential of acceleration-based monitoring for detecting structural damage by analysing changes in a bridge's dynamic characteristics (i.e. natural frequencies). These changes can serve as early indicators of deterioration, supporting proactive maintenance. However, since the study was conducted under controlled laboratory conditions, its applicability to real-world scenarios remains influenced by environmental factors, particularly temperature fluctuations. To enhance reliability, practical implementation in the case study bridges should incorporate temperature-normalized frequency tracking. Furthermore, while this study focused on







frequency changes as a damage proxy, future research should explore mode shape variations for a more comprehensive assessment.







References

- [1] DEWESoft, "DEWESoft Structural Health Monitoring Solution." Accessed: Feb. 21, 2025. [Online]. Available: https://dewesoft.com/applications/structural-health-monitoring
- [2] DEWESoft, "DEWESoft IOLITEI 3xMEMC-ACC." Accessed: Feb. 21, 2025. [Online]. Available: https://dewesoft.com/products/iolitei-3xmems
- [3] DEWESoft, "Dewesoft ARTeMIS OMA software." [Online]. Available: https://dewesoft.com/blog/announcing-the-new-dewesoft-artemis-oma-solution